

# Freezing and clustering transitions for penetrable spheres

C. N. Likos,<sup>1</sup> M. Watzlawek,<sup>2</sup> and H. Löwen<sup>1,2</sup>

<sup>1</sup> *Insitut für Festkörperforschung, Forschungszentrum Jülich GmbH, D-52425 Jülich, Germany*

<sup>2</sup> *Institut für Theoretische Physik II, Heinrich-Heine-Universität Düsseldorf,  
Universitätsstraße 1, D-40225 Düsseldorf, Germany*

(published in Phys. Rev. E **58**, 3135 (1998))

## Abstract

We consider a system of spherical particles interacting by means of a pair potential equal to a finite constant for interparticle distances smaller than the sphere diameter and zero outside. The model may be a prototype for the interaction between micelles in a solvent [C. Marquest and T. A. Witten, J. Phys. France **50**, 1267 (1989)]. The phase diagram of these penetrable spheres is investigated using a combination of cell- and density functional theory for the solid phase together with simulations for the fluid phase. The system displays unusual phase behavior due to the fact that, in the solid, the optimal configuration is achieved when certain fractions of lattice sites are occupied by more than one particle, a property that we call ‘clustering’. We find that freezing from the fluid is followed, by increasing density, by a cascade of second-order, clustering transitions in the crystal.

PACS: 64.70.Dv, 61.20.Gy, 61.20.Ja

## I. INTRODUCTION

Much of our current understanding of the liquid-solid transition from a microscopic point of view is based on the density-functional theory of inhomogeneous liquids [1–3]. This approach allows, in principle, the systematic calculation of the phase diagram of any system, once the pair potential between its constituent particles is given. A number of pair interactions of variable ‘hardness’ (hard spheres, inverse-power, Yukawa etc.) have been studied, yielding the phase coexistence between a fluid phase, which is stable up to moderate densities, and a crystal which is stable at higher densities. For most of the systems which have been considered in the literature, the assumed pair interaction between particles has the property that it grows as the distance between the particles decreases, and diverges at zero separation. These are the usual, *unbounded* interactions. For such interactions, a whole mechanism of liquid-state integral equation theories has been developed which allows one to calculate with a high degree of accuracy the structure and thermodynamics of the fluid phase, which is in turn a necessary ingredient in any density-functional treatment of the freezing transition.

Much less is known about interactions which are *bounded*, i.e. they allow the particles to ‘sit on top of each other’, imposing only a finite energy cost for a full overlap. This is natural since a true, microscopic interaction always forbids overlaps. However, the situation may be different if, e.g., one considers the ‘potential of mean force’ between two polymeric coil centroids in a good solvent, as suggested many years ago by Stillinger [4]. The two centroids may coincide without this resulting into a forbidden configuration. Stillinger thus introduced the ‘Gaussian core model’, consisting of particles that interact by means of a pair potential  $\phi(r) = \phi_0 \exp(-r^2/\sigma^2)$ , where  $r$  is the interparticle distance,  $\phi_0$  is an energy scale and  $\sigma$  is a length scale. This model and its phase diagram have been examined in Refs. [4,5], following an approach based on general mathematical properties particular to the Gaussian potential and on computer simulations, for a review see Ref. [6].

In this paper we also consider a bounded potential, albeit an apparently simpler one. We take an interaction between spheres which is simply equal to some positive constant if there is any overlap between them and zero otherwise. The study of such a model is not of purely academic interest; a few years ago, Marquest and Witten [7] suggested that interaction potentials qualitatively similar to a step function are expected for micelles in a solvent. We study the phase diagram of this model by using standard techniques (integral equation theories for the fluid and a cell model for the solid), also combined with computer simulations. We find, on the one hand, that the boundedness of the interaction makes the standard integral equation theories inadequate to accurately describe the dense liquid phase of the system. On the other hand, the fact that the interaction is constant, brings about a novel possibility for the crystal to lower its free energy, namely the formation of groups of two or more particles (‘clusters’) occupying the same lattice site, a property that we call *clustering*. As a result, there are second-order clustering transitions within the region of the phase diagram occupied by the solid.

The rest of the paper is organized as follows: in section II we present our approach for the fluid phase and in section III for the solid phases. The results are combined in section IV where we present the phase diagram of the model. Finally, in section V we summarize and conclude.

## II. PENETRABLE SPHERE MODEL: THE FLUID PHASE

We consider a model of penetrable spheres, whose interactions are described by the pair potential:

$$\phi(r) = \begin{cases} \varepsilon & 0 \leq r < \sigma; \\ 0 & \sigma < r, \end{cases} \quad (2.1)$$

where  $\sigma$  is the diameter of the spheres and  $\varepsilon$  is the height of the energy barrier ( $\varepsilon > 0$ ). The packing fraction  $\eta$  and reduced temperature  $t$  are defined as:

$$\eta = \frac{\pi}{6}\rho\sigma^3; \quad t = \frac{k_B T}{\varepsilon}, \quad (2.2)$$

where  $\rho$  is the number density,  $T$  is the temperature and  $k_B$  is Boltzmann's constant.

Clearly, at zero temperature the model reduces to the hard sphere (HS) potential. The first task is to investigate the structure and thermodynamics of the fluid state. In a theoretical approach to the problem, typically one of the various approximate liquid-state integral equation theories is employed, which yields the radial distribution function  $g(r)$  of the fluid together with the direct correlation function  $c(r)$  related to  $g(r)$  by means of the Ornstein-Zernicke (OZ) relation [8]:

$$g(r) - 1 = c(r) + \rho \int c(|\mathbf{r} - \mathbf{r}'|)[g(r') - 1]d\mathbf{r}'. \quad (2.3)$$

Another exact relation connecting  $g(r)$  with  $c(r)$  reads as:

$$g(r) = \exp\{-\beta\phi(r) + g(r) - 1 - c(r) - B(r)\}, \quad (2.4)$$

where  $B(r)$  is the so-called bridge function [9], the sum of all elementary diagrams that are not nodal. Since  $B(r)$  is not known, the various approximate liquid-state integral equation theories can be regarded as approximations of this quantity. In this way, an additional equation or 'closure' involving only  $g(r)$  and  $c(r)$  is supplemented to the OZ-relation and the system becomes solvable.

The simplest and most frequently employed theories are the Hypernetted Chain (HNC) and Percus-Yevick (PY) schemes which, however, due to their approximate character lack thermodynamic consistency; the 'pressure' and 'compressibility' routes to the liquid free energy yield different results. In the HNC, one simply sets  $B(r) = 0$ , obtaining the closure:

$$g(r) = \exp\{-\beta\phi(r) + g(r) - 1 - c(r)\}. \quad (2.5)$$

On the other hand, the Percus-Yevick closure can be seen as a linearized version of the HNC regarding the term  $g(r) - 1 - c(r)$  in the exponential and reads as:

$$g(r) = e^{-\beta\phi(r)}[g(r) - c(r)], \quad (2.6)$$

corresponding to the following approximation for the bridge function:

$$B_{PY}(r) = [g(r) - c(r)] - 1 - \ln[g(r) - c(r)]. \quad (2.7)$$

There have been various attempts to improve the above approximations and to come up with a manageable theory which would also overcome the problem of thermodynamic inconsistency mentioned above. Among the most popular are the Modified HNC (MHNC) approach of Rosenfeld and Ashcroft [9] and the theory of Rogers and Young (RY) [10]. In the latter, one replaces the exact relation (2.4) above by the closure:

$$g(r) = \exp\{-\beta\phi(r)\} \left[ 1 + \frac{\exp\{\gamma(r)f(r)\} - 1}{f(r)} \right], \quad (2.8)$$

where  $\gamma(r) = g(r) - c(r) - 1$  and  $f(r)$  is a ‘mixing function’ depending on a single parameter  $\zeta$  and taken to have the form:

$$f(r) = 1 - \exp(-\zeta r). \quad (2.9)$$

The parameter  $\zeta$  is determined in such a way that thermodynamic consistency is achieved. The nomenclature ‘mixing function’ comes from the fact that the RY-closure provides a means of interpolation between the PY- and HNC-closures.

In order to obtain a comparison and test the performance of integral equations, we have also performed standard Monte-Carlo simulations [11] in the constant  $NVT$ -ensemble. All runs were performed in a cubic box containing 500 particles and using periodic boundary conditions. We calculate the radial distribution function  $g(r)$  as well as the structure factor  $S(k)$  ‘on the flight’.

For  $t = 0$ , where our model reduces to hard spheres, the PY solution is analytic and is known to describe the pair structure of the HS fluid quite well. As a first step, therefore, we have solved the PY closure for finite temperatures as well. In Fig. 1 we show results for  $g(r)$  and in Fig. 2 for the structure factor  $S(k)$  for  $t = 0.2$  and packing fraction  $\eta = 0.3$  in comparison with simulation. In Fig. 3 we compare the  $g(r)$ ’s for the same temperature and  $\eta = 0.5$ . As can be seen, for the lower density,  $g(r)$  is reproduced quite well by the PY-closure outside the core. However, inside the core the simulation shows a tendency of  $g(r)$  to grow towards the origin, which is *not* reproduced by the PY-result. The growth of  $g(r)$  towards the origin can be simply understood as follows: since the interaction is such that it does not impose any additional penalty for full sphere overlaps (in comparison with partial ones), as the density grows there is an increasing tendency of the particles to form clusters in which more and more spheres ‘sit on top of each other’. In this way, more space is left free for the remaining clusters and the optimal configuration is achieved. The discrepancies between the PY and the true results are not dramatic for  $\eta \lesssim 0.3$  and this limit grows with decreasing temperature. Moreover, the discrepancies in the structure factor are much less pronounced than those for the distribution function. However, the differences become really spectacular as the packing fraction grows. The PY-closure is inadequate to reproduce the accumulation of spheres on top of each other and brings about a radial distribution function that is quite wrong at high densities.

The failure of the PY-closure to describe the very dense liquid at finite temperatures is not a surprise; after all, it is known that PY works best for hard, short-range interactions like hard spheres. Thus, we resorted to the HNC as a possible solution. In Fig. 1 we show the comparison of the HNC- $g(r)$  with simulation for the data point  $t = 0.2$ ,  $\eta = 0.3$ . As can be seen, now the penetration towards the origin is *overestimated*. In fact, this feature

becomes more and more pronounced as  $\eta$  grows and, as a result, the HNC fails to converge any more for  $\eta \gtrsim 0.6$  at  $t = 0.1$ . We can qualitatively understand the overestimation of  $g(r)$  inside the core by the HNC as follows: it is well-known that the bridge function is a positive-definite quantity [9] (although this has not been strictly proven, it turns out to be true in almost all cases) and thus it plays the role of an ‘effective repulsive interaction’. Then the HNC, by setting  $B(r) = 0$  everywhere, gives rise to a  $g(r)$  which is too high. For the case of an unbounded interaction which diverges at the origin, inaccuracies in the approximation of  $B(r)$  especially for low  $r$  where this function is relatively large, cause no serious problems. Indeed, referring to Eq. (2.4) we see that if  $\phi(r) \rightarrow \infty$  as  $r \rightarrow 0$ , then the interaction dominates in the exponential and sends  $g(r) \rightarrow 0$  for short separations. But in our case where  $\phi(r)$  remains finite for all  $r$ , an accurate knowledge of the bridge function is *essential* in order to bring about a sensible theory for this system.

The Rogers-Young closure provides a more sophisticated approximation for  $B(r)$ . We have attempted, therefore, to solve this closure but again we ran into difficulties: no self-consistent solution could be found for  $\eta \gtrsim 0.45$  for  $t = 0.1$ . Moreover, the results for the lower values of  $\eta$  were very similar to the PY-ones. Further attempts to modify and improve the RY closure did not yield the desired agreement with the simulations. We do not expect that any other of the standard closures will be of much use either, for the reasons described above: in the formulation of all approximate liquid-state theories it is assumed (explicitly or implicitly) that the strongly repulsive interaction simply forbids close approaches between particles, so that there exists some (generally temperature- and density-dependent) distance  $r_0$ , such that for  $r < r_0$  the radial distribution function  $g(r)$  vanishes. Here, the situation is quite the opposite: the interaction is such that it *favors* close approaches (in fact: full overlaps) at high density. Thus, we have decided to resort entirely to computer simulations in order to calculate the structure and thermodynamics of the fluid phase at high densities.

There are two ways or ‘routes’ to evaluate the excess free energy of a fluid from a simulation. The density route or ‘ $\eta$ -route’ consists of performing a series of simulations at *fixed* temperature but for increasingly high densities. Once the radial distribution function  $g(r; \eta)$  has been calculated, the form of the interaction at hand implies that the excess pressure is related to the ‘jump’ of  $g(r)$  by the equation:

$$\frac{\beta P_{ex}}{\rho} = 4\eta[g(\sigma^+; \eta) - g(\sigma^-; \eta)], \quad (2.10)$$

where  $g(\sigma^\pm; \eta)$  is the value of  $g(r)$  immediately outside/inside the core. Then, the excess free energy per particle is obtained by:

$$\frac{\beta F_{ex}(\eta)}{N} = \int_0^\eta \frac{\beta P_{ex}}{\rho} \frac{d\eta'}{\eta'}. \quad (2.11)$$

Another way to calculate the excess free energy is by the so-called temperature route or ‘ $t$ -route’. Here, one makes use of the thermodynamic identity relating the excess energy per particle,  $U_{ex}/N \equiv u_{ex}(\beta)$  and the reduced excess free energy per particle,  $\beta F_{ex}/N \equiv \beta f_{ex}(\beta)$  at *fixed* density:

$$u_{ex}(\beta) = \frac{\partial[\beta f_{ex}(\beta)]}{\partial \beta}, \quad (2.12)$$

to express the latter as an integral from  $T = \infty$  (where  $u_{ex}$  vanishes) to the considered value of the temperature:

$$\beta f_{ex}(\beta) = \int_0^\beta u_{ex}(\beta') d\beta'. \quad (2.13)$$

Thereby, a series of simulations is performed at fixed  $\eta$  but at successively decreasing temperatures. For each temperature, the value of the internal energy is measured and at the end the integral of Eq. (2.13) is performed. Notice that for the interaction at hand, the evaluation of the internal energy in a simulation is particularly simple; denoting by  $N_\sigma$  the average number of particles lying within distance  $\sigma$  from a given particle during the simulation, one simply has:

$$u_{ex}(\beta) = \frac{1}{2} \varepsilon N_\sigma(\beta). \quad (2.14)$$

If one envisions a two dimensional  $\eta$ - $t$  plane, then the  $\eta$ -route corresponds to a horizontal path and the  $t$ -route to a vertical path along this plane. If neither of the two paths crosses any phase boundaries along its way from its starting point to its end, then the values obtained for the excess free energy using either route should be *identical*. If, on the other hand, one (or more) phase boundaries are encountered along the way, then differences will occur. We have, therefore, performed simulations for various different temperatures and density ranges to check this agreement and to use the results as a first diagnostic tool for possible phase transformations on the system. Results for temperatures  $t = 0.1, 0.2$  and  $1.0$  are shown in Figs. 4(a), (b) and (c) respectively. As can be seen, the two routes yield identical results (within ‘experimental’ errors) for the highest temperature, up to  $\eta = 1.8$ . However, for the two lowest temperatures, discrepancies start to appear, for  $t = 0.1$  at about  $\eta = 0.5$  and for  $t = 0.2$  at about  $\eta = 0.7$ . As this is a clear indication of a phase transition located in the neighborhood of these  $\eta$ -values, neither the  $\eta$ - nor the  $t$ -route results can be considered as reliable estimates of the free energy of the system for values of  $\eta$  exceeding the above. However, they can be used in conjunction with our theoretical results for the free energy of the *crystal* phase in order to draw some general conclusions regarding the *topology* of the phase diagram, on the one hand, and to trace it out in more detail on the other. These considerations are presented in the section IV.

### III. THE SOLID PHASES

#### A. General considerations

In the solid phase the one-particle density  $\rho(\mathbf{r})$  is position-dependent, a property that characterizes the crystal as an inhomogeneous phase. In the last twenty years, a common theoretical tool which provides for a satisfactory treatment of the freezing transition has been density-functional theory (DFT). In DFT, the crystal is viewed as a spatially inhomogeneous fluid and the properties of the homogeneous phase are used to evaluate the free energy of a candidate crystalline structure, for a review see [2,3]. Among the most popular versions of DFT is the modified weighted density approximation (MWDA) of Denton and Ashcroft [12], which has been proven to be quite reliable for the case of the hard-sphere freezing transition.

In common applications of the MWDA, the one-particle density of the candidate crystal structure is modeled as a sum of normalized Gaussians centered around lattice sites, and the width (localization) of the Gaussians is used as a variational parameter until a minimum of the free energy is found. Typically, one makes in the MWDA the assumption that there is just one particle per lattice site. This is manifested in the usual parametrization for the one particle density mentioned above which reads as:

$$\rho(\mathbf{r}) = \left(\frac{\alpha}{\pi}\right)^{3/2} \sum_{\{\mathbf{R}\}} \exp[-\alpha(\mathbf{r} - \mathbf{R})^2], \quad (3.1)$$

where  $\{\mathbf{R}\}$  denotes the set of Bravais lattice vectors and  $\alpha$  is the localization parameter. We call the version of the MWDA where the above assumption is made the constrained-MWDA.

In principle, one would like to have at hand the possibility of treating the average site occupancy as an *additional* parameter in the theory. Then, the restricted parametrization (3.1) above, must be replaced by the more general expression:

$$\rho(\mathbf{r}) = x \cdot \left(\frac{\alpha}{\pi}\right)^{3/2} \sum_{\{\mathbf{R}\}} \exp[-\alpha(\mathbf{r} - \mathbf{R})^2], \quad (3.2)$$

where  $x$  stands for the average site occupancy and is to be treated as a variational quantity. For a HS-crystal (and in general for all diverging potentials which do not allow multiple occupancy), it is natural to expect  $x \leq 1$ . For the interaction at hand, this general parametrization is quite essential, if DFT is to be used, for the following reason: as the density of the crystal is increased beyond the close-packing limit of the considered structure, it is expected that it will be favorable for the system to form fractions of pairs, triplets etc. Indeed, whereas for a crystal with single occupancy the energy cost per site above the close packing limit is equal to one-half of the number of nearest neighbors, formation of a number of pairs brings about a much lower cost, simply equal to the number of paired sites. At the same time, by pairing the lattice constant ‘opens up’ and overlaps between nearest neighbors are avoided. The tendency for the formation of composite particles, or ‘clusters’ is also manifested already in the fluid, through the dramatic increase of the liquid-state  $g(r)$  towards the origin mentioned in the previous section.

The difficulty we are faced with, however, is that a free minimization of the MWDA-functional does *not* yield a physically acceptable value for  $x$  for the case of hard spheres. Indeed, it has been found [13] that the minimum of the unconstrained MWDA occurs for a site occupancy  $x = 1.31$ , an obvious physical impossibility for hard spheres. It follows then that the results of a free minimization of the MWDA-functional cannot be trusted, at any temperature. If, on the other hand, the general parametrization given by Eq. (3.2) above is maintained, but the domain of acceptable solution for  $x$  is restricted by hand to  $0 \leq x \leq 1$ , then the value  $x = 1$  is obtained as the minimum. Hence, the *constrained* MWDA gives quite reliable results for the entropic free energy of a HS crystal.

Clearly, the possibility of clustering appears as a mechanism for the lowering of the free energy of the crystal mainly for packing fractions exceeding the close-packing limit  $\eta_{CP}$ ; at low temperatures (with which we are concerned here), we can still use the constrained MWDA for  $\eta < \eta_{CP}$  and obtain information about the structure of solids with single occupancy. We carried out the MWDA calculation for temperatures  $0.0 \leq t \leq 0.3$ , using the

PY-results as input for the fluid structure and free energy. The advantage of the MWDA is that the solid is mapped onto an effective liquid having a ‘weighted packing fraction’  $\hat{\eta}$  which is much lower than  $\eta$  of the solid [12], typically  $\hat{\eta} \approx 0.30$ . The necessary ingredients for the MWDA are the values of the structure factor  $S(|\mathbf{K}|; \hat{\eta})$  of the liquid at the nonzero reciprocal lattice vectors  $\mathbf{K}$  of the crystal and the free energy per particle of the fluid again at packing fraction  $\hat{\eta}$  [12]. For such low packings, the PY-solution is reliable, as can be seen from Fig. 2 for the structure factor and from Figs. 4(a), (b), where we show the free energy curves obtained from the compressibility route of the PY-solution, demonstrating that they run very close to the simulation results for low packings. We found that for all temperatures, the solid free energies were indistinguishable from the HS ( $t = 0$ ) result, demonstrating that the structure of the solids below close packing, even at finite temperatures is identical to the HS-solid, i.e. the particles avoid any overlap. We will make use of this preliminary result shortly. However, for the study crystals with packing fraction exceeding  $\eta_{CP}$ , the MWDA is unsuitable for the reasons explained above, and we have to resort to a different approach.

### B. A cell model for the clustered solids

Let us consider, to begin with, a HS-solid of  $N$ -particles (HS diameter  $\sigma$ , mass  $m$ ) enclosed in volume  $\Omega$ , having packing fraction  $\eta$ , and site occupancy equal to unity. The partition function  $Q_N(\eta)$  is given by:

$$Q_N(\eta) = \left( \frac{4\pi}{h^3} \int p^2 e^{-\beta p^2/(2m)} dp \right)^N \times \frac{1}{N!} \int_{\Omega} d\mathbf{r}_1 d\mathbf{r}_2 \cdots d\mathbf{r}_N e^{-\beta V(\mathbf{r}_1, \mathbf{r}_2, \dots, \mathbf{r}_N)} \\ \equiv \Theta_N \times Z_N(\eta), \quad (3.3)$$

where  $h$  is Planck’s constant,  $\Theta_N$  is the kinetic and  $Z_N$  the configurational part of the partition function. For the evaluation of the latter, we adopt the cell model [14–17] which exploits the picture of particle in a solid as being confined in cells of cages formed by the neighboring ones from which it cannot escape. We emphasize here that we employ the cell model only as an intermediate step in order to establish a relation between the free energy of a clustered crystal and that of a HS crystal and not as a computational tool in order to actually calculate these quantities. The packing fraction  $\eta$  and the candidate crystal structure determine the volume of the cell, also called free volume  $v_f(\eta)$ . Then, the particles in the solid can be treated as distinguishable. Since within the cell the Boltzmann factor is unity, the configurational partition function is given by:

$$Z_N(\eta) = \left( \int_{v_f(\eta)} d\mathbf{r} \right)^N = v_f^N(\eta). \quad (3.4)$$

Strictly speaking, the expression above provides only a lower bound to the true partition function of the crystal [18,19].

Combining Eqs. (3.3), (3.4) above, we obtain the free energy per particle of a HS-crystal having packing fraction  $\eta$  and site occupancy one, as:

$$\frac{\beta F_{\text{HS}}(\eta)}{N} \equiv f_0(\eta) = -\ln \left[ \frac{v_f(\eta)}{\Lambda^3} \right], \quad (3.5)$$



where  $\Lambda \equiv (2\pi mk_B T/h^2)^{1/2}$  is the thermal de Broglie wavelength.

Let us now proceed in an analogous way for the general case  $t \neq 0$ . As mentioned above, we expect the formation of doublets, triplets etc. in the crystal. Clearly, as the density is increased, more and more complicated composites will appear (quadruplets, quintuplets etc.) To keep the discussion simple (and the theory computationally manageable) we restrict ourselves here to clusters up to triplets only.

Let us then consider  $N$  particles in a crystal with  $N_s$  sites. Of these  $N_s$  sites,  $N_1$  are occupied by a single particle,  $N_2$  by pairs and  $N_3$  by triplets. We set:

$$\frac{N_1}{N_s} \equiv s, \quad \frac{N_2}{N_s} \equiv z \quad \text{and} \quad \frac{N_3}{N_s} \equiv w. \quad (3.6)$$

Clearly,  $s + z + w = 1$  and  $N = (1 + z + 2w)N_s$ . The result of the formation of composites is that the ‘clustered solid’ has a lattice constant which corresponds not to  $\eta$  but to a new, *effective* packing fraction  $\gamma$  which is lower and related to  $\eta$  by:

$$\gamma = \frac{\eta}{1 + z + 2w}. \quad (3.7)$$

The idea is that the system will find it favorable to create as many clusters as possible so as to bring about an effective packing  $\gamma$  which is below  $\eta_{CP}$ . This way, the energy cost comes entirely from the sphere overlaps in the clusters themselves; otherwise, the lattice cell is now large enough, so that the expensive, multiple overlaps with the neighbors are avoided. This assumption is corroborated by the MWDA-results for the single-occupied solids below  $\eta_{CP}$ . Indeed, it was found that, for low temperatures and  $\eta < \eta_{CP}$ , the system behaves essentially as a HS-crystal. Hence, our model for the clustered solid is the following: enough clusters are formed so that the effective packing fraction  $\gamma$  is always below  $\eta_{CP}$  and, once this has been achieved, each object occupying a lattice site (being a single particle or a composite) acts as a hard sphere with respect to any other object occupying a neighboring site.

With these assumptions in mind, we now proceed with a cell model for the clustered solid. The free volume  $v_f$  is now dictated by the packing fraction  $\gamma$ . Each site occupied by a pair brings about an energy cost  $\varepsilon$  and each site occupied by a triplet a cost  $3\varepsilon$ . Taking into account the indistinguishability of the particles in the clustered sites, we can now write down an expression the partition function of our clustered crystal which, at this stage, does *not* include the entropy of mixing:

$$Q_N(\eta, t) = \Theta_N \times \left[ \int_{v_f(\gamma)} d\mathbf{r} \right]^{N_1} \times \left[ \frac{e^{-\beta\varepsilon}}{2!} \int_{v_f(\gamma)} d\mathbf{r} \int_{v_f(\gamma)} d\mathbf{s} \right]^{N_2} \times \left[ \frac{e^{-3\beta\varepsilon}}{3!} \int_{v_f(\gamma)} d\mathbf{r} \int_{v_f(\gamma)} d\mathbf{s} \int_{v_f(\gamma)} d\mathbf{t} \right]^{N_3}. \quad (3.8)$$

Using the relation  $N = N_1 + 2N_2 + 3N_3$ , performing the volume integrals above and taking the logarithm, we obtain:

$$-\frac{\ln Q_N(\eta, t)}{N} = -\ln \left[ \frac{v_f(\gamma)}{\Lambda^3} \right] + \left( \frac{N_2 + 3N_3}{N} \right) t^{-1} + \frac{N_2}{N} \ln 2 + \frac{N_3}{N} \ln 6. \quad (3.9)$$

The first term is, according to Eq. (3.5), nothing else but  $f_0(\gamma)$ , the free energy of a HS-crystal having packing fraction  $\gamma$ . The above expression is not yet the free energy of the

clustered crystal as it does not include the ‘mixing-entropy’ contributions arising from all the possible ways of choosing the  $N_2$  and  $N_3$  sites which are occupied by clusters. This mixing entropy is simply:

$$S_{mix} = k_B \ln W, \quad (3.10)$$

where  $W$  is precisely the number of ways of choosing  $N_2$  and  $N_3$  sites out of  $N_s$  for the multiple occupancies. It is straightforward to show that:

$$W = \frac{N_s!}{N_2!N_3!(N_s - N_2 - N_3)!}. \quad (3.11)$$

Finally, the  $z$ - and  $w$ -dependent *variational* expression for the free energy per particle of a solid with clusters is given by:

$$\frac{\beta \tilde{F}(\eta, t; z, w)}{N} \equiv \tilde{f}(\eta, t; z, w) = -\frac{\ln Q_N(\eta, t)}{N} - \frac{S_{mix}}{k_B N}. \quad (3.12)$$

Collecting the results from Eqs. (3.6)-(3.9) and (3.11) above, we finally obtain:

$$\begin{aligned} \tilde{f}(\eta, t; z, w) = & f_0 \left( \frac{\eta}{1+z+2w} \right) + \left( \frac{z+3w}{1+z+2w} \right) t^{-1} + \left( \frac{z \ln 2 + w \ln 6}{1+z+2w} \right) + \\ & \frac{1}{1+z+2w} [z \ln z + w \ln w + (1-z-w) \ln(1-z-w)]. \end{aligned} \quad (3.13)$$

The quantities  $z$  and  $w$  are variational parameters, as there are no chemical potentials controlling the site occupancy, hence the free energy per particle of the solid is given by:

$$f(\eta, t) = \min_{\{z, w\}} \tilde{f}(\eta, t; z, w). \quad (3.14)$$

In our considerations we have examined both the fcc- and bcc-solids, finding that the fcc is favorable always. So we restrict the discussion to this structure only. For the fcc,  $\eta_{CP} = 0.74$ . For the free energy per particle of the HS-solid,  $f_0$ , at packing fraction  $\gamma = \eta/(1+z+2w) < \eta_{CP}$  we use the results from the constrained-MWDA. An important result from the MWDA is that the fcc HS-solid is *mechanically unstable* below  $\eta = 0.46$ , i.e. the MWDA-free energy cannot be minimized by a nonzero value of  $\alpha$  if the packing fraction is below the value mentioned above. We have, thus, imposed an artificially high (practically infinite) value for the function  $f_0(\eta)$  for  $\eta < 0.46$  and proceeded with the numerical minimization. The latter must be performed in the triangular domain which is enclosed in the  $z$ - $w$  plane by the boundaries:  $0 \leq z \leq 1$ ;  $0 \leq w \leq 1$ ; and  $z + w \leq 1$ .

### C. Comparison with simulations

In order to check the reliability of the fraction of doubly occupied lattice sites  $z$  as obtained from the above described theoretical model, we performed a numerical calculation of the free energy  $\tilde{F}$  of the fcc solid at fixed temperature  $t = 0.1$  and fixed particle volume fraction  $\eta = 0.8$ , where the theory predicts  $w = 0$ , i.e. there are only singlets and doublets in

the crystal. For that purpose, we took advantage of a thermodynamic integration method initially introduced by Frenkel and Ladd [20,21]. In this Monte Carlo method, the free energy of the investigated system is calculated by transforming the system reversibly into a harmonic Einstein crystal of the same crystal symmetry, whose free energy  $F^{Ein}$  is known analytically. The crystal symmetry of the reference crystal is simply characterized by the zero temperature lattice sites of the  $N$  simulated particles  $\{\mathbf{R}\}_0^N = (\mathbf{R}_{0,1}, \dots, \mathbf{R}_{0,N})$ . A throughout extensive description of the method can be found in Ref. [22].

In our specific use of this method, we choose the lattice sites  $\mathbf{R}_0^N$  of the reference harmonic crystal to be partially doubly occupied, i.e. we set  $\mathbf{R}_{0,i} = \mathbf{R}_{0,j}$  for some randomly chosen particle numbers  $i$  and  $j$ . We do not allow three particles to have the same reference crystal position. So, the reference crystal structure is characterized by its crystal symmetry (chosen to be fcc in our case), its particle volume fraction  $\eta$ , and its fraction of doubly occupied lattice sites  $z$ . For fixed  $\eta$  and  $z$ ,  $\tilde{F}$  could then be calculated as described in detail in Refs. [21,22]. We performed calculations for various pairing fractions  $z$ , ranging from 0.35 to 0.80, fixing the temperature at  $t = 0.1$  and the density at  $\eta = 0.8$ . In all simulations, the number of particles was between 500 and 700, therefore finite size effects could be neglected.

Since our Monte Carlo simulations were always performed for one specific realization of the singlet-and-doublet fcc solid, we had to add the mixing entropy  $S_{mix}$  [as given by Eqs. (3.10) and (3.11)] to our Monte Carlo free energy results. In principle, in the Monte Carlo simulations, the system was free to explore the configuration space associated with the various possible realizations of the fcc solid, since we did not restrict the particle coordinates to distinct regions in the simulation box. However, this would have required very long simulation runs since very large mean-square displacements of the particles would have been needed. Since in our simulations the mean-square displacements of the particles were in the order of the lattice spacings, we had to take into account the mixing entropy  $S_{mix}$ .

In Fig. 5 we show our Monte Carlo results for the free energy of the fcc solid with singly- and doubly-occupied sites including the mixing entropy  $S_{mix}$ , as a function of  $z$  for fixed  $t$  and  $\eta$ . Also shown is the corresponding results of our above described theoretical model [i.e. from Eq. (3.13) with  $w = 0$ .] Obviously, the agreement of the pairing fractions  $z_{min}$ , where the free energy of the fcc solid achieves a minimum is very good. We have also done the same check at different  $\eta$ -values, obtaining similar agreement; thus, the theory described above provides a reliable method for the calculation of the free energy of the crystals.

#### D. Results of the variational calculation

We now present in detail the results obtained from the theory in the range of thermodynamic parameters  $0 \leq t \leq 0.3$  and  $\eta \leq 2.2$ . First, we introduce a terminology to characterize the various types of fcc-solids with respect to the fractions of sites occupied by clusters, as follows:

- (i) S-solid if  $s = 1$ ,  $z = w = 0$ ;
- (ii) SP-solid if  $0 < s < 1$ ,  $0 < z < 1$  and  $w = 0$ ;
- (iii) P-solid if  $s = 0$ ,  $z = 1$  and  $w = 0$ ;
- (iv) PT-solid if  $s = 0$ ,  $0 < z < 1$  and  $0 < w < 1$ ;
- (v) SPT-solid if  $0 < s < 1$ ,  $0 < z < 1$  and  $0 < w < 1$ , and
- (vi) T-solid if  $s = z = 0$ ,  $w = 1$ .

These are the six types of solids that come out of the minimization. In Fig. 6 we show the dependence of  $s$ ,  $z$  and  $w$  on the fcc-packing fraction  $\eta$  for  $t = 0.05$ . The typical scenario that materializes, at least for temperatures  $t \lesssim 0.1$  is the following: for packing fractions  $\eta \lesssim \eta_{CP}$ , we have the usual S-solid, as there is no particular gain for clusters to be formed. At higher densities, pairs start to appear and an SP-solid is formed. The pair fraction grows with density at the expense of the singly-occupied sites. Depending on the temperature, the fraction of pairs may reach the value unity at about  $\eta \approx 2\eta_{CP}$  before any triplets appear, thus forming a P-crystal; this happens for  $t \lesssim 0.05$ . For higher temperatures, triplets appear while both  $s$  and  $z$  are nonzero, thus giving rise to a SPT-solid. By further increase of the density, the single-occupancy sites disappear altogether and a PT-solid emerges. Then, the pairs start being replaced by triplets completely and a T-solid takes the place of the PT-solid.

As shown in Fig. 6, the fractions of multiply occupied sites approach zero in a continuous way. Thus, we are having a sequence of *second-order clustering transitions* in the solid which gets more and more complicated as the packing fraction grows. Whether all this sequence of transitions will actually appear in the phase diagram depends also on the competition with the liquid free energy. The full phase diagram, including the freezing transition, is discussed in the following section.

#### IV. THE PHASE DIAGRAM

In this section we determine the low-temperature phase diagram of the system, putting together the results obtained for the free energy of the solid, obtained by the procedure described previously, and those for the fluid free energy coming from the simulations. A representative case for  $t = 0.1$  is shown in Fig. 7. The first question to be addressed is the topology of the phase diagram, in particular the possibility of the existence of *reentrant melting*, i.e. a remelting of the solid at higher densities. This is a realistic possibility which in fact materializes for the bounded Gaussian potential of Stillinger [4–6].

Referring to Fig. 7, we see that if the  $\eta$ -route result for the is taken as the ‘true’ liquid free energy, then we would have indeed reentrant melting; in fact, for this temperature the solid would be marginally stable at  $\eta \approx 1.0$ , i.e.  $t = 0.1$  would be very close to a ‘maximum freezing temperature’ above which no thermodynamically stable solids would exist. However, were this to be the case, then the  $t$ -route to the fluid free energy would have crossed no phase boundaries along its way. Thus, the  $t$ -route would have given the true fluid free energy at high packings and this, in turn, ought to lie below the solid free energy, consistently with the reentrant-melting scenario. Obviously, this is not the case. This leads us to the conclusion that there is no reentrant melting, at least not in the range of densities considered here. Instead, there is freezing into a fcc-solid, followed by a cascade of clustering transitions as described in the previous section.

The coexistence densities for the freezing transition are determined by performing a common-tangent construction on the fluid- and solid-free energy curves. As mentioned previously, none of the  $\eta$ - or  $t$ -route curves can be considered as the ‘true’ free energy of the fluid beyond the point where they start to diverge from each other. However, the  $\eta$ -route curve is in a way ‘more wrong’ than the  $t$ -route curve in the sense that it yields, at high densities, fluid free energies which are lower than their solid counterparts and this leads to

the contradiction explained above. Thus, the correct free energy of the fluid must follow a curve which is identical to the simulation results up to the point where the two routes agree (and where the liquid is stable) and then it must cross the solid free energy and run above it (and thus the liquid is there metastable). In this sense, the fluid free energy is ‘closer’ to that obtained by the  $t$ -route than the one obtained from the  $\eta$ -route. Therefore, we have performed the common-tangent construction using the  $t$ -route result for the fluid. As the lower end of the common tangent ends up lying in the region where the  $t$ -route results are indeed reliable, the precise shape of the liquid free energy curve for densities *beyond* freezing is immaterial.

From the more quantitative point of view, the fact that the coexistence region lies *precisely* in the domain where the  $\eta$ - and  $t$ -routes yield results that begin to diverge is an independent confirmation for the theoretical approach we employed for the solid. Indeed, this discrepancy is the signature of a phase transition which now comes about to be located in the right place by means of a completely independent theoretical approach for the crystal. The same agreement was found at all temperatures we considered.

Putting now everything together, we trace out the liquid-solid coexistence curves as well as the boundaries of the second-order transitions between the crystals with the different types of clustering. The phase diagram obtained in this way is shown in Fig. 8. The region of stability of the T-phase is artificially enlarged. The reason is that, in order to determine with accuracy the stability for a given type of clusters, at least the next type of cluster must be put into the theory, i.e. quadruplets for the T-solid etc. As this is an increasingly complicated procedure, we have not done this here. However, in view of the results already obtained, we expect that the solid will proceed with more and more clustering at increasing density, thus giving rise to a quite interesting phase diagram.

## V. DISCUSSION AND CONCLUSIONS

We have considered a toy model of penetrable spheres characterized by an interaction which imposes a constant energy cost if there is any overlap between the spheres (no matter how strong) and zero otherwise. Although the model is quite simple, the form of the interaction, which favors full overlaps between the particles, brings about quite a few interesting features. As a first remark, we have found an inadequacy of the traditional liquid-state integral equation theories to describe in a satisfactory way the high-density fluid phase of the system. We believe that this shortcoming can be traced back to the inaccuracies in the estimation of the bridge function, inherent in all approximate closures. Such inaccuracies are not dramatic if we are dealing with a unbounded interaction. In those cases, the different closures give results which differ on the amount of structure of, say, the radial distribution function  $g(r)$  outside some effective core where  $g(r)$  vanishes. However, since the bridge function  $B(r)$  attains its highest values *precisely* for  $r \rightarrow 0$ , if the bare interaction is not strong enough to dominate over the bridge function, then inaccuracies in the determination of the latter become really crucial. Thus, it is not surprising that in our case the problem becomes more severe as the density grows (because then  $B(r)$  grows as well) and/or as the temperature is raised (because then the bare interaction  $\beta\phi(r)$  diminishes.)

To the best of our knowledge, the only other bounded interaction for which an attempt has been made to trace out the phase diagram is the Gaussian model of Stillinger [4–6]. In

that case, it was found that the model displayed reentrant melting. In Ref. [4], some general criteria for the mathematical form of the interaction were laid down and it was stated that for any pair potential meeting those criteria, reentrant melting behavior had to be expected. These conditions are: (i) the interaction must be bounded at the origin; (ii) it must vanish strongly enough at infinity to be integrable and (iii) it must be differentiable at least four times. Our interaction satisfies these requirements, with the exception of (iii) since it has a singularity at  $r = \sigma$  and it is not differentiable there. However, this does not constitute a serious violation as one could easily imagine an analytic potential that would run arbitrarily close to our ‘step function’ and for that potential the results would be practically identical to the ones found here. However, another important ingredient that goes into reaching these general conclusions is the assumption that the solid (or solids of different crystal symmetry) which are ‘nested’ between the fluid at low- and high-densities have single site occupancy. We have not found reentrant melting in our case, at least for the range of densities and temperatures we considered. Although we cannot exclude this possibility at some other region of the phase diagram, we believe that the arguments of Ref. [4] do not apply to our case, precisely due to the clustering in the solid which takes place in our model. For the same reasons, our results are at odds with those of Marquest and Witten [7] who found regions of stability of the bcc- and simple-cubic structures at growing density, based on calculations of the ground-state energy, making the assumption of single occupancy in the crystal. We find instead that a cascade of second-order transitions takes place in the crystal.

## ACKNOWLEDGMENTS

We are pleased to acknowledge useful discussions with Prof. D. Frenkel and Dr. A. R. Denton. M. W. thanks the Deutsche Forschungsgemeinschaft for support within the SFB 237.

## REFERENCES

- [1] R. Evans, Adv. Phys. **28**, 143 (1979).
- [2] Y. Singh, Phys. Rep. **207**, 351 (1991).
- [3] H. Löwen, Phys. Rep. **237**, 249 (1994).
- [4] F. H. Stillinger, J. Chem. Phys. **65**, 3968 (1976).
- [5] F. H. Stillinger and T. A. Weber, J. Chem. Phys. **68**, 3837 (1978).
- [6] F. H. Stillinger and D. K. Stillinger, Physica A **244**, 358 (1997).
- [7] C. Marquest and T. A. Witten, J. Phys. France **50**, 1267 (1989).
- [8] J. P. Hansen and I. R. McDonald, *Theory of Simple Liquids*, 2nd Edition (Academic, London 1986).
- [9] Y. Rosenfeld and N. W. Ashcroft, Phys. Rev. A **20**, 1208 (1979).
- [10] F. J. Rogers and D. A. Young, Phys. Rev. A **30**, 999 (1984).
- [11] M. P. Allen and D. J. Tildesley, *Computer Simulation of Liquids* (Clarendon Press, Oxford, 1987).
- [12] A. R. Denton and N. W. Ashcroft, Phys. Rev. A **39**, 4701 (1989).
- [13] R. Ohnesorge, H. Löwen, and H. Wagner, Phys. Rev. A **43**, 2870 (1991); Europhys. Lett. **22**, 245 (1993).
- [14] A. Bonissent, P. Pieranski, and P. Pieranski, Phil. Mag. A **50**, 57 (1984).
- [15] W. W. Wood, J. Chem. Phys. **20**, 1334 (1952).
- [16] J. G. Kirkwood, J. Chem. Phys. **18**, 380 (1950).
- [17] K. W. Wojciechowski, Phys. Lett. A **122**, 377 (1987).
- [18] M. Schmidt, *Freezing in confined geometry* (Shaker Verlag, Aachen, 1997).
- [19] M. Schmidt and H. Löwen, Phys. Rev. Lett. **76**, 4552 (1996); Phys. Rev. E **55**, 7228 (1997).
- [20] D. Frenkel and A. J. C. Ladd, J. Chem. Phys. **81**, 3188 (1984)
- [21] D. Frenkel, Phys. Rev. Lett. **56**, 858 (1986)
- [22] D. Frenkel and B. Smit, *Understanding Molecular Simulation*, (Academic Press, London, 1996), Chapter 9.2.

## FIGURES

FIG. 1. Comparison of the radial distribution function  $g(r)$  as obtained from simulation, and the PY- and HNC-closures, for a system of penetrable spheres at reduced temperature  $t = 0.2$  and packing fraction  $\eta = 0.3$ .

FIG. 2. Comparison between the simulation result and the PY-closure for the structure factor  $S(k)$  at the same point as in Fig. 1.

FIG. 3. Comparison between the simulation result and the PY-closure for the function  $g(r)$  at  $\eta = 0.5$  and  $t = 0.2$ . Note the dramatic increase of  $g(r)$  from simulation inside the core. The simulation value for  $g(r)$  at  $r = 0$  is in fact equal to 18.5.

FIG. 4. Free energy densities as obtained by the  $\eta$ - and  $t$ -routes of the simulation. (a)  $t = 0.1$ ; (b)  $t = 0.2$ ; (c)  $t = 1.0$ . The solid lines in (a) and (b) denote the results obtained by using the compressibility route of the PY-solution and demonstrate that for low densities the PY-closure gives reasonable results for this quantity.

FIG. 5. The variational free energy of an fcc-solid having packing fraction  $\eta = 0.8$  at temperature  $t = 0.1$  as a function of the fraction of sites occupied by pairs.

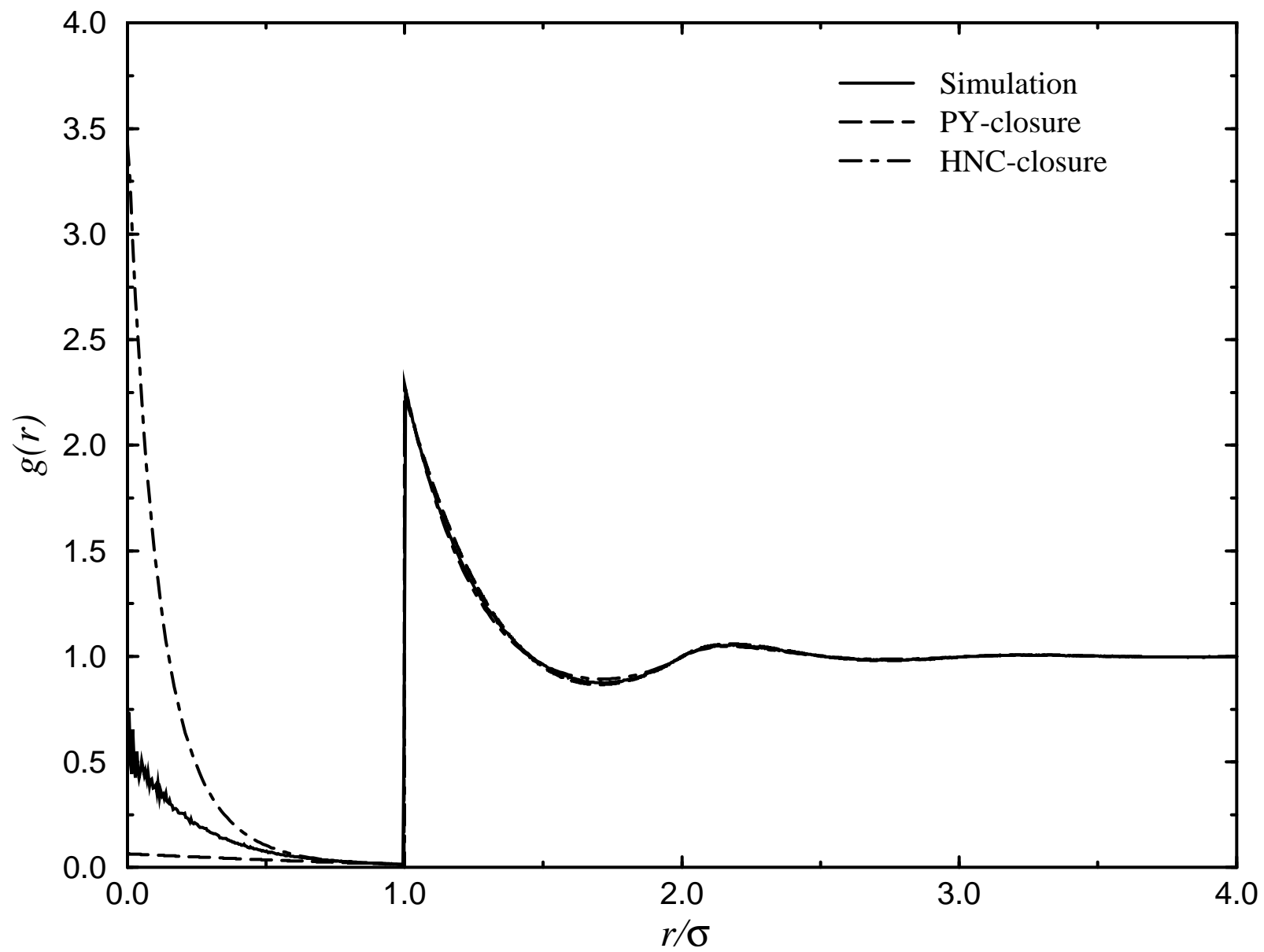
FIG. 6. The fraction of sites with single, double and triple occupancy as a function of  $\eta$  for fcc-solids at temperature  $t = 0.05$ .

FIG. 7. Free energy densities for the fluid, as obtained by using the  $\eta$ - and  $t$ -routes in the simulation and for the solid as a result of the theory. The reduced temperature is  $t = 0.1$ .

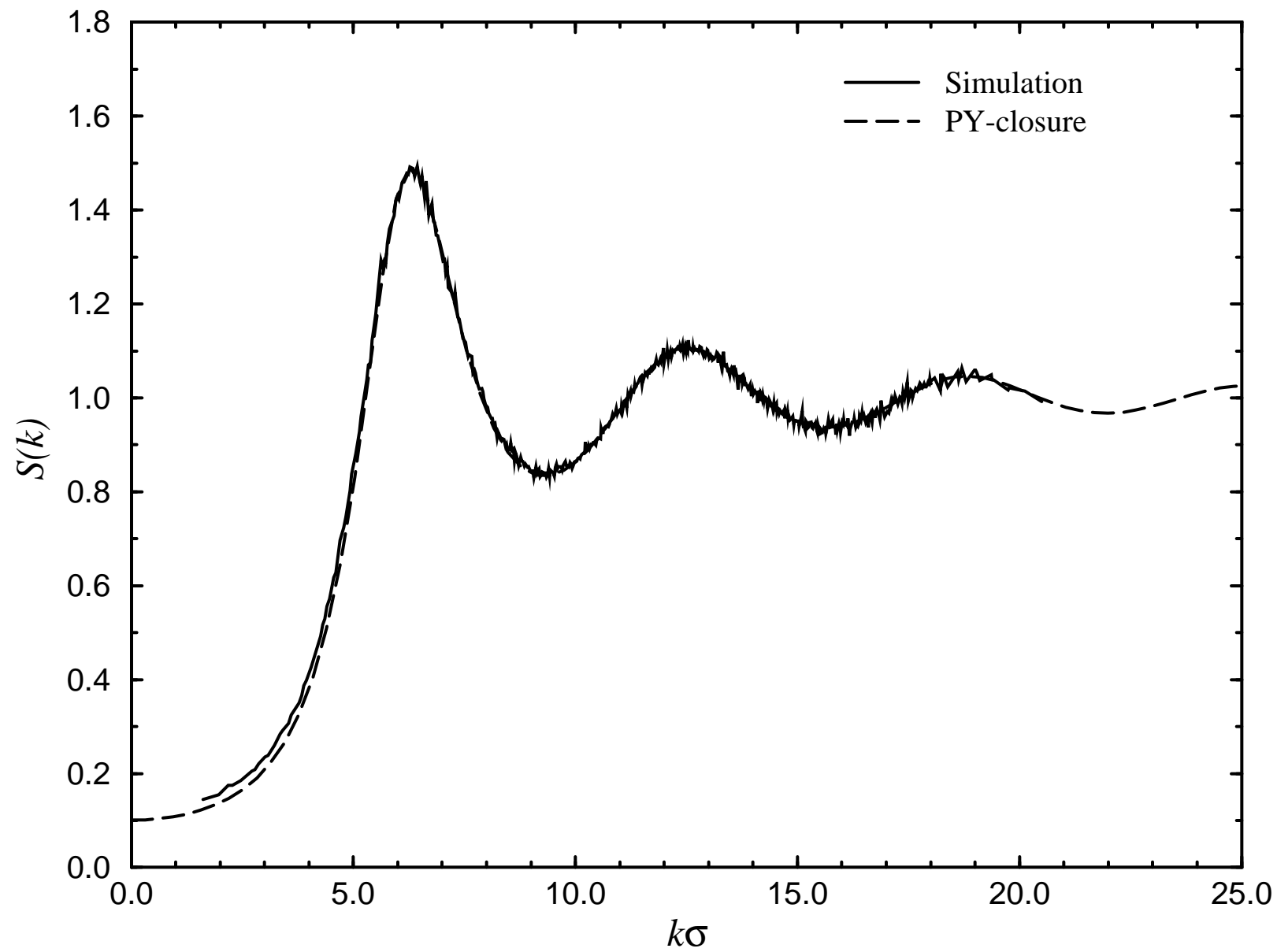
FIG. 8. The phase diagram of the penetrable sphere model. The thick lines denote the first-order freezing transition and the shaded region is the liquid-solid coexistence region. The dashed lines denote second-order clustering transitions in the solid. As explained in the text, the region of stability of the T-solid is artificially enlarged due to the lack of the possibility of formation of four-particle clusters in our theory.



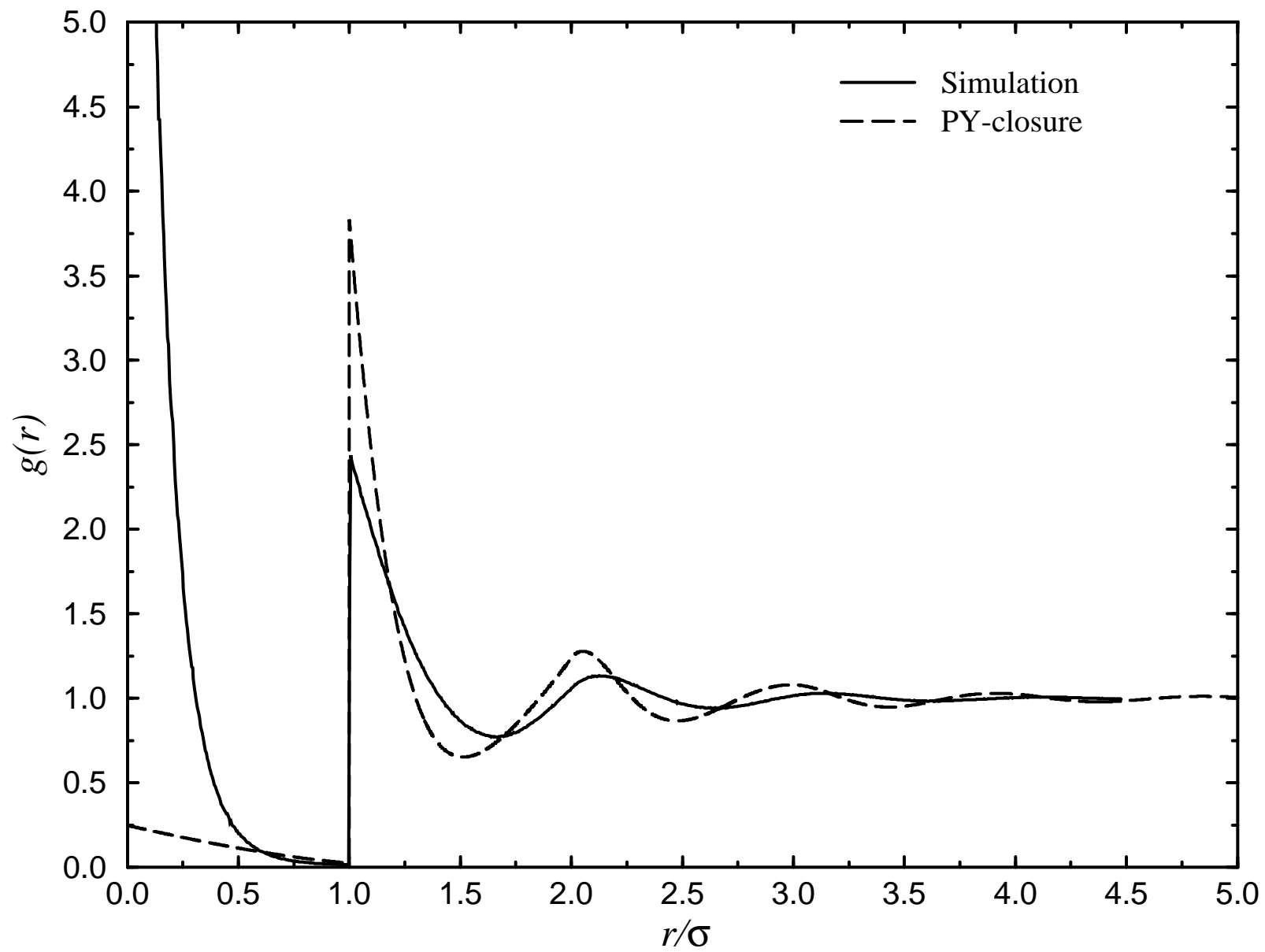
Likos, Watzlawek, and Loewen, Fig. 1



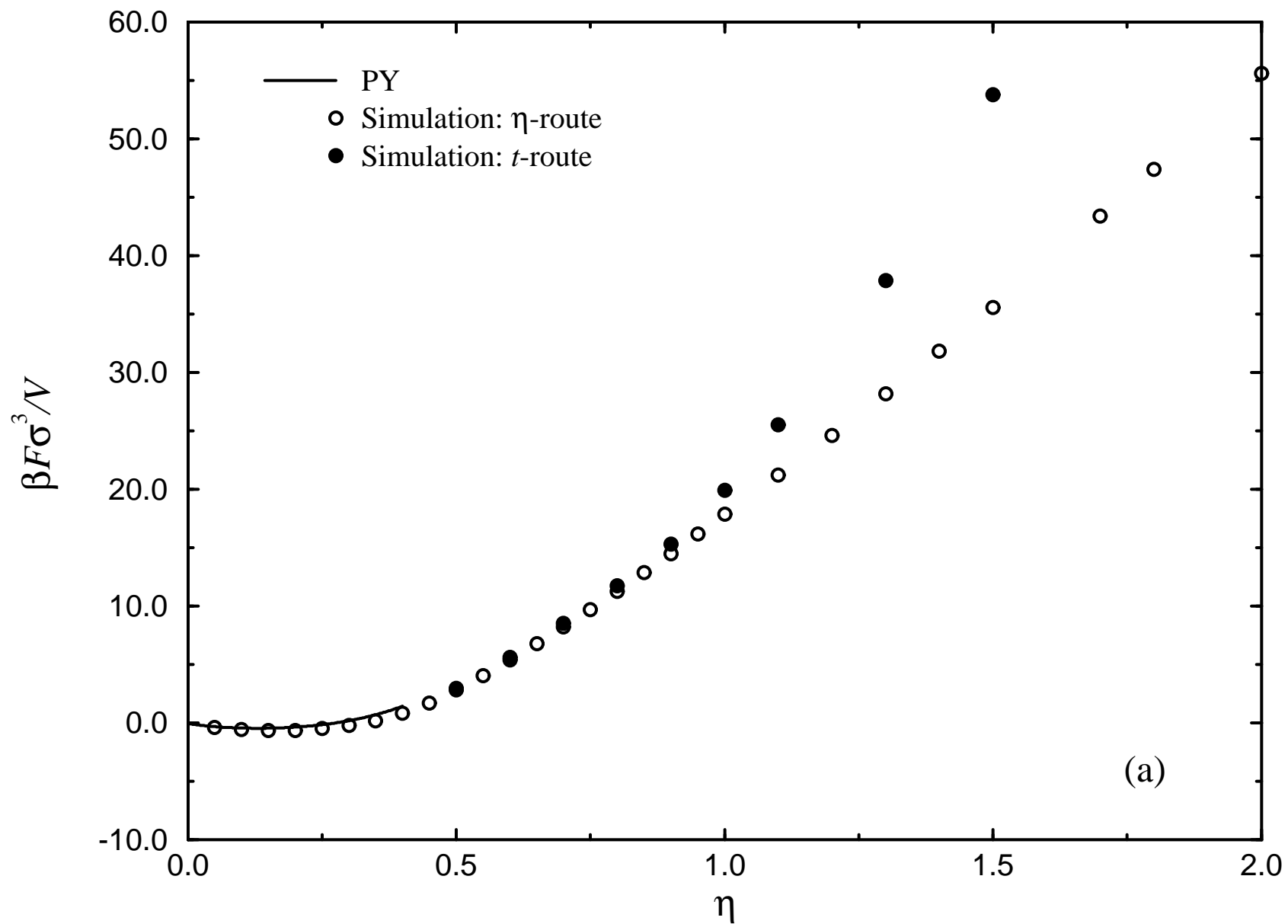
Likos, Watzlawek, and Loewen, Fig. 2



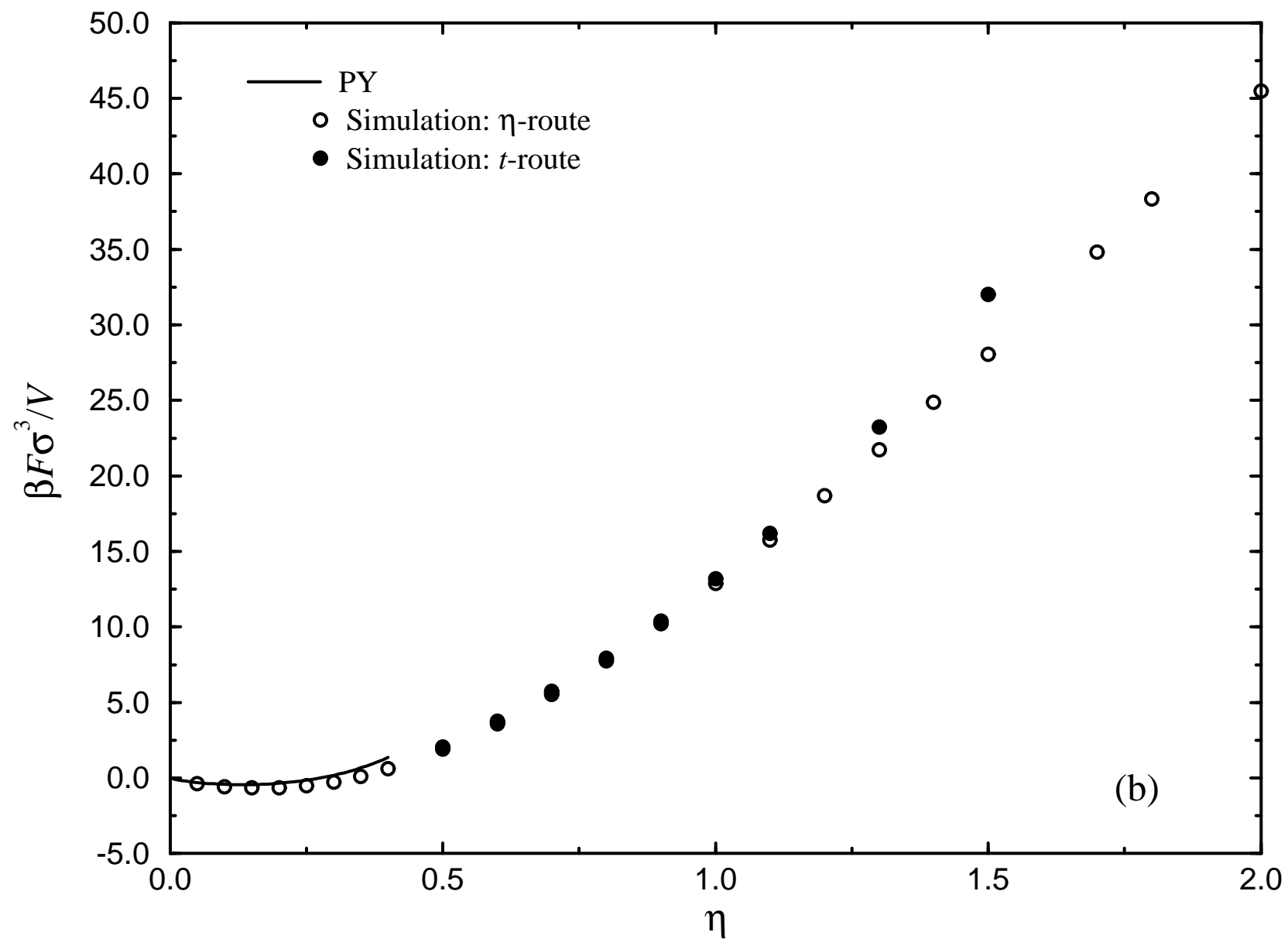
Likos, Watzlawek, and Loewen, Fig. 3



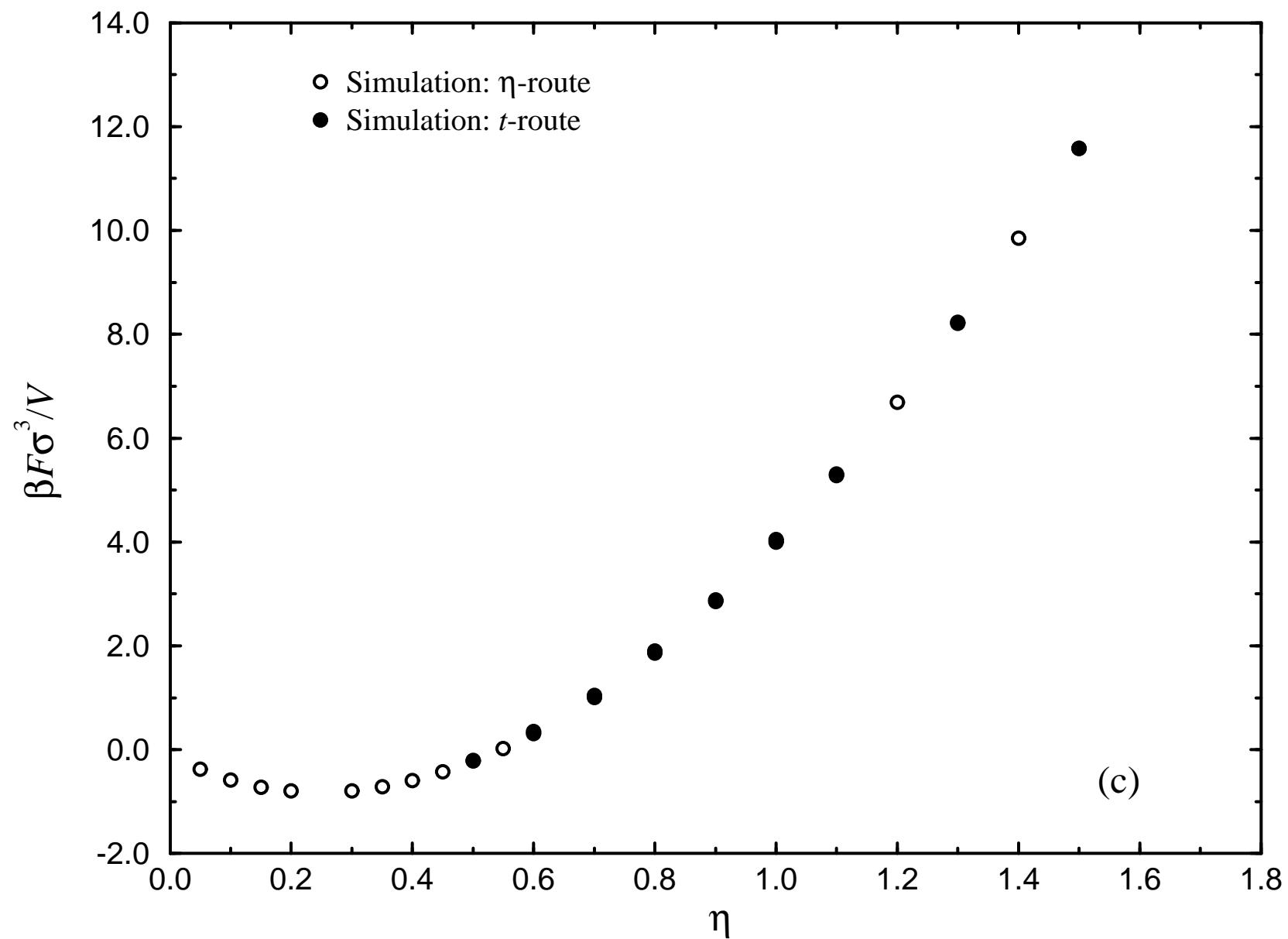
Likos, Watzlawek, and Loewen, Fig. 4(a)



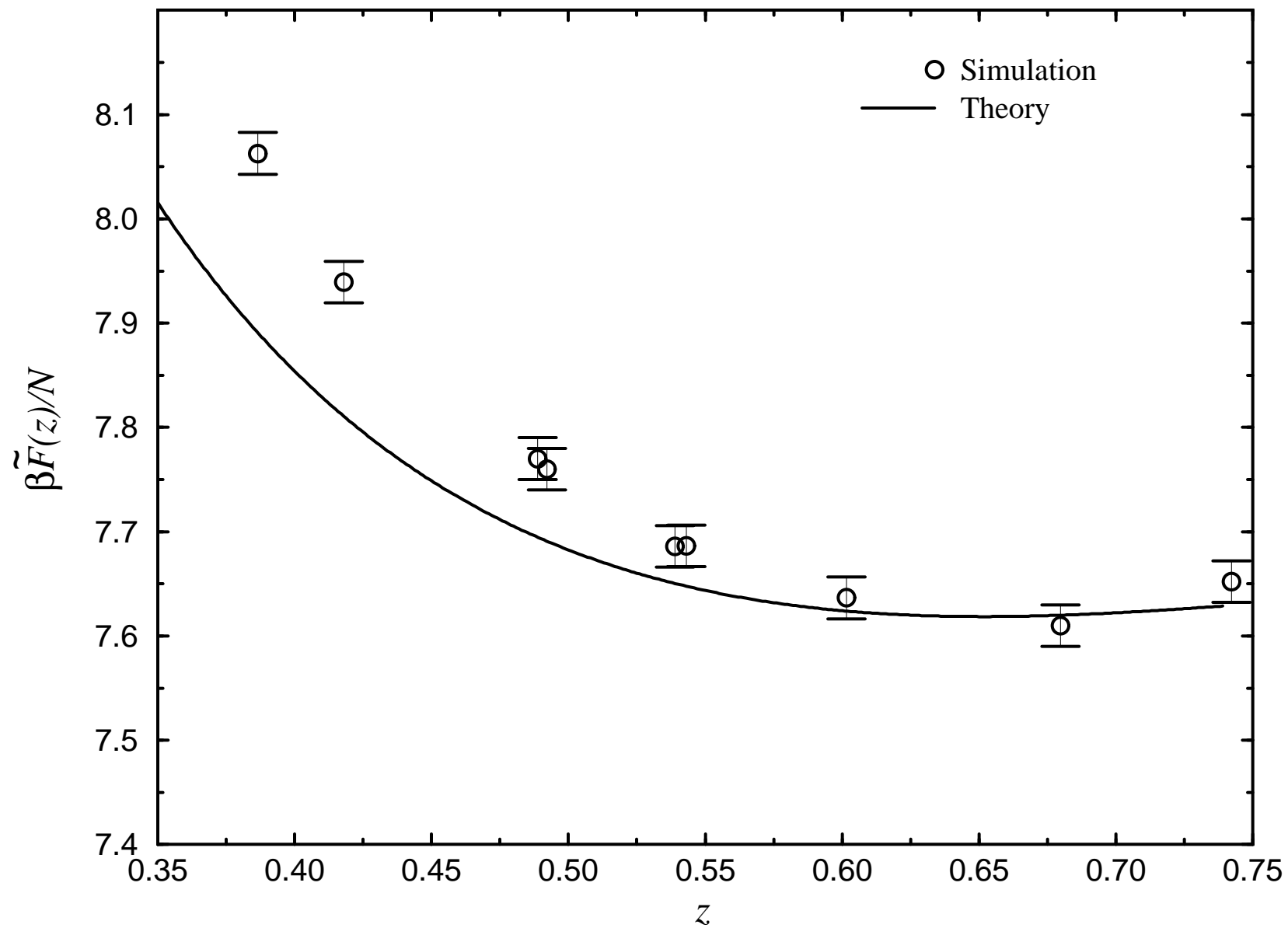
Likos, Watzlawek, and Loewen, Fig. 4(b)



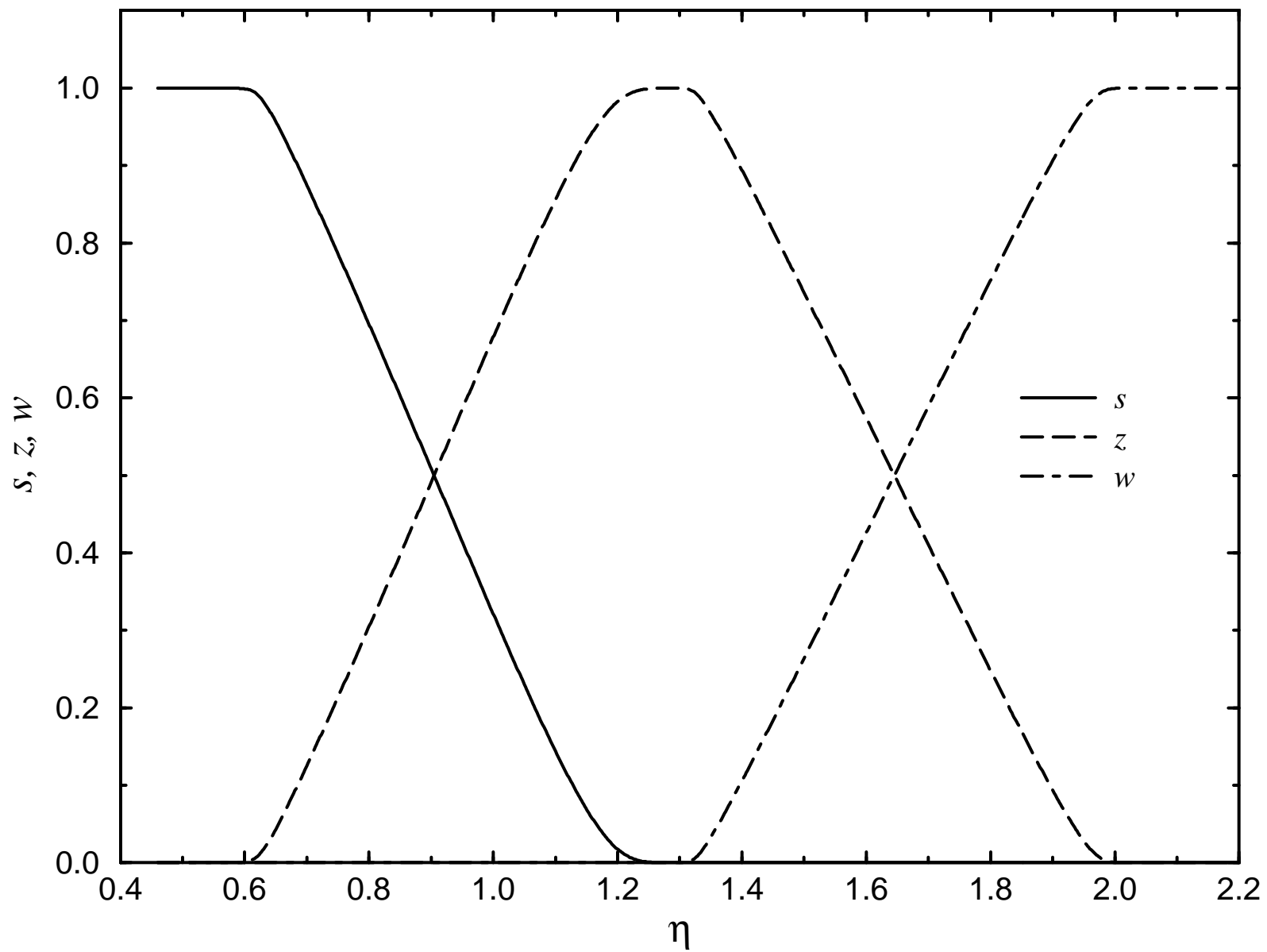
Likos, Watzlawek, and Loewen, Fig. 4(c)



Likos, Watzlawek, and Loewen, Fig. 5

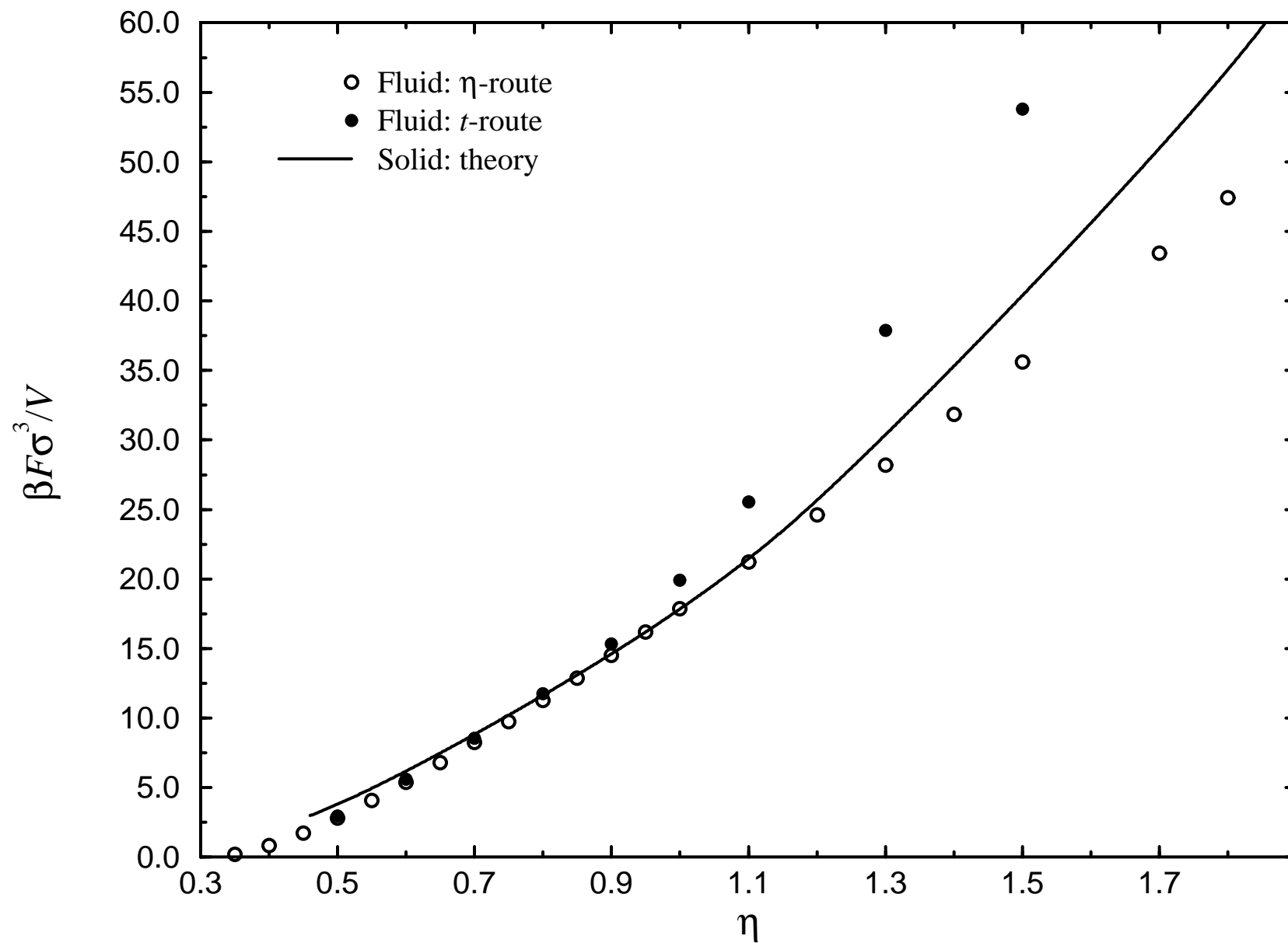


Likos, Watzlawek, and Loewen, Fig. 6





Likos, Watzlawek, and Loewen, Fig. 7



Likos, Watzlawek, and Loewen, Fig. 8

